ORIGINAL ARTICLE

Patient-specific arterial system flow oscillation

Fytanidis DK[1], Soulis JV[1], Giannoglou GD[2]

[1] Fluid Mechanics Division, School of Engineering, Democrition University of Thrace, Xanthi
[2] Cardiovascular Engineering and Atherosclerosis Laboratory, 1st Cardiology Department, AHEPA University Hospital, Medical School, Aristotle University of Thessaloniki, Thessaloniki,
Greece

Abstract

Background: Atherosclerosis formation depends on the biomechanical blood flow properties. The temporal variation during the cardiac cycle has been proposed as a decisive atherogenic factor. Patient-specific (complex configuration) of the vessel promotes flow disturbances. The present study analyses the factors simulating pulsatile blood flow in the human arterial system using patient-specific geometry.

Methods: With the aid of numerical techniques, we examine the relation between time-Averaged Wall Shear Stress (AWSS), time-Averaged Wall Shear Stress Vector (AWSSV), Oscillatory Shear Index (OSI) and Relative Residence Time (RRT).

Results: The velocity vector oscillates and at the same time alters its direction in places with low AWSS values. Low AWSS and high OSI values do not always collocate. AWSSV tends to alter its values, compared to AWSS, in regions where AWSS is low. RRT present high values in areas with low AWSS. The inverse proportionality relation between RRT and AWSSV is established.

Conclusions: Regional differences between AWSS magnitude, OSI and RRT, may answer the question as to where atherosclerotic lesions predominately develop and progress at specific aortic regions. This analysis gives information for deeper understanding of the atherosclerosis mechanisms. Hippokratia 2014; 18 (2):162-165.

Keywords: Oscillatory shear index, relative residence time, patient-specific arterial system analysis

Corresponding Author: Johannes V. Soulis, BSc, MSc, PhD, Fluid Mechanics Division, Faculty of Engineering, Demokrition University of Thrace, Vas. Sofias 12, 67100 Xanthi, Greece, tel: +302541079617, e-mail: jvsoulis@med.auth.gr

Introduction

The blood flow properties, such as Wall Shear Stress (WSS) and macromolecules transport through human arteries are shown to be important factors for endothelial dysfunction[1,2]. WSS affects arterial wall properties such as hydraulic conductivity[3,4], filtration velocity[5] and net endothelial permeability[6]. Complex geometry and pulsating flow in the human arterial system lead to substantial spatial and temporal alterations in WSS. Research[7] associates atherosclerotic lesions with low WSS locations.

The importance of low WSS and high Oscillatory Shear Index (OSI) in atherosclerosis is reported by Chatzizisis et al[8]. Regional variations of WSS and OSI in the aortic arch was examined by flow sensitive 4D MRI, Frydrychowicz et al[9] reporting that biomechanical flow parameters WSS and OSI may help explaining where lesions initiate and substantially develop in the aorta. Other attempts, aim to choose the optimal biomechanical flow parameter for the prediction of plaque location[10]. The advances of computerized image processing technology and the improved resolution of medical imaging processes, forced research to use more realistic geometries. Thus, "patient-specific" geometry is used in several works; suggestively[11-13]. A general fully computerized algorithm of 3D geometry reconstruction using CT or MRI images data for biomedical applications was published[14].

In the current work a semi-automatic computerized methodology was used to reproduce the 3D geometry of a healthy middle-aged male's arterial system and a computational model is applied to elucidate the relation between the transient biomechanical flow properties, namely the time-Averaged Wall Shear Stress (AWSS), the time-Averaged Wall Shear Stress Vector (AWSSV), the OSI and the, recently introduced, Relative Residence Time (RRT).

Methods

The commercial software Materialise Mimics is used to reconstruct the 3D arterial system geometry processing 2D CT digital image. 2D images were imported in "dicom" format. Part of the patient-specific aorterial system geometry is shown in Figure 1. The final smoothed geometry was imported into the computational grid generator. Details of the patient-specific arterial system (aortic

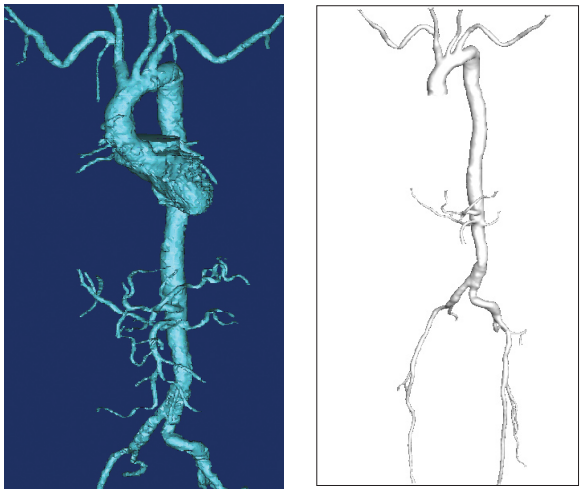

Figure 1: Constructed (left) patient-specific cardiovascular system and numerically tested (right) arterial system.

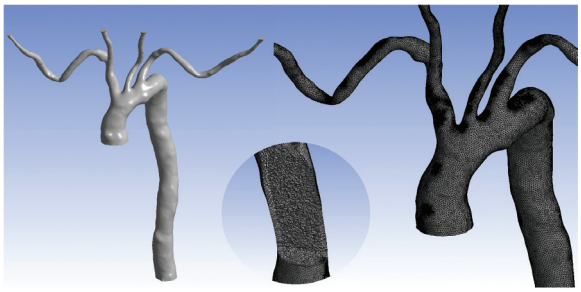

Figure 2: Patient-specific aortic arch geometry.

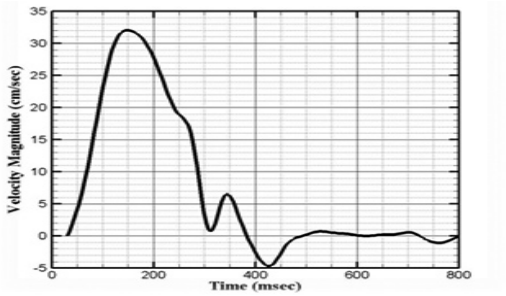

Figure 3: The waveform at the inlet of the patient-specific aortic arch.

arch) geometry and its computational grid are shown in Figure 2.

The governing flow equations, namely Navier-Stokes, are solved for incompressible, isothermal and laminar flow, using the finite-volume method provided by the commercial solver ANSYS Fluent 14.0[15] (ANSYS, Inc. Southpointe, Canonsburg, PA, USA).

Details can be found in the paper by Soulis et al (2002)[2]. The blood is treated as non-Newtonian fluid obeying to the power law[16].

Figure 3 shows the applied velocity pulsewave at inlet[17]. The pulse period of this waveform is 800.0 msec. Outflow discharges for the problem were calculated using a slightly modified version of the Murray's Law[18]. Mesh independence study was performed using 2.6, 4.7 and 11.1 million cells grids.

For the applied geometry, the 4.7 million cells grid test case gave mesh-independent solution for WSS and OSI values. Moreover, 8 cardiac cycles were simulated to avoid period dependencies. The WSS (N/m^2), AWSS (N/m^2), AWSSV (N/m^2) and OSI are defined as,

$$WSS=\tau=\left[\mu\ \dot{S}\right]\dot{S} \quad AWSS=\frac{1}{T}\int_0^T\left|\overrightarrow{WSS}\right|dt \quad AWSSV=\frac{1}{T}\left|\int_0^T\overrightarrow{WSS}dt\right| \quad OSI=0.5\times\left(1-\frac{\left|\int_0^T\overrightarrow{WSS}dt\right|}{\int_0^T\left|\overrightarrow{WSS}\right|dt}\right)$$

μ (kg/m-s) is the blood molecular viscosity, $\dot{S}$ is the strain rate (1/sec), $\left|\overrightarrow{WSS}\right|$ is the instantaneous WSS magnitude and T (sec) is the pulse period. The OSI value can vary from 0, for no-cyclic variation of WSS vector, to 0.5, for 180.0^o deflection of WSS direction. Flow pulsatility alone, a) gives rise to flow reversal and b) is insensitive to WSS magnitude. Low WSS may or may not be affected by the flow pulsatility. Under the same inlet waveform conditions, strongly oscillatory flows can exhibit the same OSI as very slow flows. Thus, the OSI misses information regarding the above flow conditions and needs modification in order to capture the atheromatic flow regions i.e. low WSS and high OSI at the same site of the arterial system. To overcome the above difficulties the Relative Residence Time (RRT) is introduced[19] as, $RRT\sim\left[(1-2.0xOSI)\times AWSS\right]^{-1}$. The proportionality of the above equation is of relative importance since the results are presented as normalized ones. Thus, the OSI modifies the AWSS effects on the RRT at a given region of the endothelium. Henceforth, the RRT parameter includes effects of both OSI and AWSS.

Results and Discussion

The AWSS (N/m^2) contours for the arterial system are shown in Figure 4. In the ascending aorta, aortic arch (ascending-descending aorta) and descending aorta (part of the arterial system). The AWSS values vary between 0.2 N/m^2 and 3.0 N/m^2. High AWSS is encountered at the convex parts of the curved flow regions. Low AWSS develops at the concave parts of the curved flow regions. Furthermore, the flow within the aortic branches is strongly dependent upon the geometry of the branch and its particular

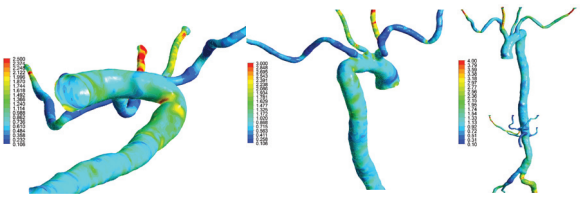

Figure 4: AWSS (N/m^2) of the patient-specific arterial system.

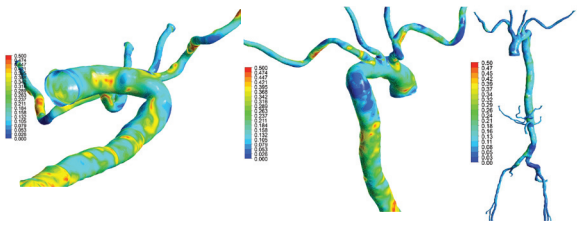

Figure 5: OSI of the patient-specific arterial system.

placement within the aorta. Thus, the right common carotid artery exhibits increased AWSS throughout the cardiac pulse. In contrast, the right subclavian branch exhibits particularly low AWSS. Always, low AWSS is major factor contributing to the onset and development of atherosclerosis. The OSI reveals the WSS magnitude of the vector inversion during the cardiac pulsewave. Contours of the aortic arch and of the arterial system are shown in Figure 5. OSI values in the main artery i.e. in the ascending aorta, aortic arch and descending aorta (arterial system), vary between 0.0 and 0.50. High OSI values are encountered at the lower part of the outer descending aorta region. Furthermore, high OSI values develop at the mid-convex part of the ascending-descending aorta. Low OSI develops at the upper concave part of the descending region aorta. This region shows high AWSS and AWSSV values. Typical relationship between OSI and AWSS and OSI and AWSSV over the entire arterial surfaces is shown in Figure 6, respectively. Increasing OSI values coexist with decreasing AWSS. Also, the OSI attains higher values in regions where AWSSV magnitude is low. A typical RRT contour of the arterial system (aortic arch) is shown in Figure 7 whereas its relation with AWSS is shown in Figure 8. RRT attains high values in arterial system regions where low AWSS appears.

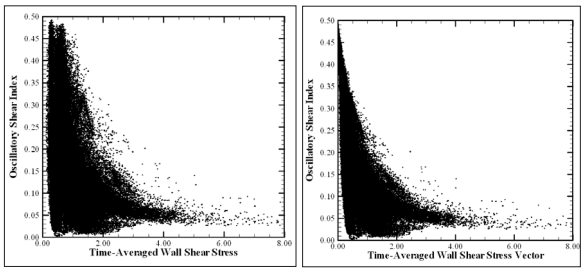

Figure 6: OSI versus AWSS (N/m^2) (left) and OSI versus AWSSV (N/m^2) (right) of the patient-specific arterial system.

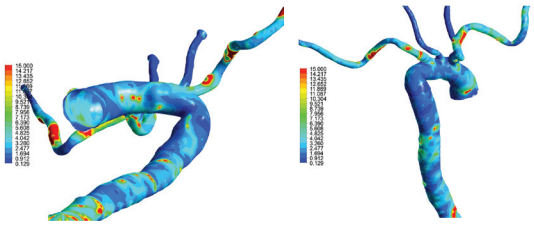

Figure 7: RRT of the patient-specific arterial.

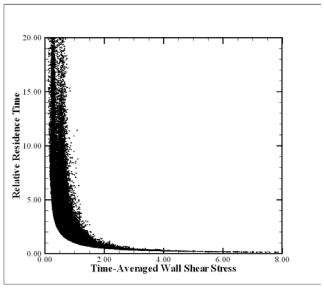

Figure 8: RRT versus AWSS (N/m^2) of the patient-specific arterial system.

The purpose of this study was to perform hemodynamic analysis of human arteries (patient-specific), particularly the aorta, and to analyze the relationships between AWSS, AWSSV, OSI and RRT. Numerical results[20], among numerous others, suggest that low WSS and high OSI tend to cause wall thickening along the inferior wall of the healthy aorta and the anterior wall of the brachiocephalic artery. In general, low AWSS and high OSI are considered to be susceptible to intimal thickening. It is apparent that as the AWSS lowers the OSI increases. This output agrees with previous works' results in patient-specific aortic arch simulation of pulsatile blood flow using Large Eddy Simulation[21] as well as with the results of blood flow in pulmonary arteries[22]. OSI has negative correlation with AWSS and AWSSV having a Pearson coefficient values of r= -0.465 ($p<0.01$), (high AWSS-low OSI).

In order to monitor WSS vector's oscillating behaviour the OSI and RRT are shown in Figure 9.

Results indicate that aorta regions of high OSI do not

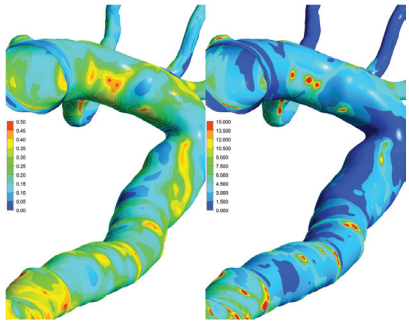

Figure 9: OSI (left) and RRT (right) distribution in patient-specific aorta.

always collocate with regions of low AWSS. As the OSI increases the AWSS and AWSSV attain low values. This relation clearly shows that high oscillation of WSS vector occurs in low AWSSV regions. Pearson coefficient between AWSSV and OSI equals r= -0.606 ($p<0.01$). On the other hand, the differences between AWSS and AWSSV tend to vary in areas of low AWSS, less than 2.5~3.0 (N/m^2). Larger discrepancies between AWSS and AWSSV appear in areas of even lower AWSS, 0.0-2.5 (N/m^2), presenting a Pearson correlation coefficient 0.976 ($p<0.01$). Statistical analysis of data result into an exponential fitting curve,

$$RRT = f(AWSS) = \frac{1.5244}{AWSS^{1.308}} = \frac{\alpha}{AWSS^{\beta}} .$$

The R-squared of the above equation is 0.8132 ($p<0.01$) (α=1.5244 and β=1.308). This statistically significant correlation shows that AWSS strongly affects RRT spatial distribution.

Conclusion

Using numerical techniques we examine the spatial distribution and the relation between the biomechanical flow parameters AWSS, AWSSV, OSI and RRT. Lower AWSS and AWSSV values give rise to higher OSI values. The velocity vector oscillates and at the same time

alters its direction in places. Low AWSS and high OSI values do not always collocate. AWSSV gives rise to high oscillation in regions with either low AWSS or high OSI. RRT attains high values in areas where AWSS is low. The inverse proportionality relation between RRT and AWSS is established. Regional differences between WSS magnitude, OSI and RRT, may answer the question as to where atherosclerotic lesions predominately develop and progress at specific aortic regions.

Conflict of interest

Authors declare no conflict of interest.

References

1. Ethier CR. Computational modeling of mass transfer and links to atherosclerosis. Ann Biomed Eng. 2002; 30: 461-471.
2. Soulis JV, Giannoglou GD, Papaioannou V, Parcharidis GE, Louridas GE. Low-Density Lipoprotein concentration in the normal Left Coronary Artery tree. Biomed Eng Online. 2008; 7: 26.
3. Sill HW, Chang YS, Artman JR, Frangos JA, Hollis TM, Tarbell JM. Shear stress increases hydraulic conductivity of cultured endothelial monolayers. Am J Physiol. 1995; 268: H535-H543.
4. Sun N, Wood NB, Hughes AD, Thom SAM, Xu XY. Fluid-wall modelling of mass transfer in an axisymmetric stenosis: effects of shear-dependent transport properties. Ann Biomed Eng. 2006; 34: 1119-1128.
5. Soulis JV, Fytanidis DK, Papaioannou VC, Giannoglou GD. Wall shear stress on LDL accumulation in human RCAs. Med Eng Phys. 2010; 32: 867-877.
6. Stangeby DK, Ethier CR. Computational analysis of coupled blood-wall arterial LDL transport. J Biomech Eng. 2002; 124: 1-8.
7. Caro CG, Fitz-Gerald JM, Schroter RC. Atheroma and arterial wall shear. Observation, correlation and proposal of a shear dependent mass transfer mechanism for atherogenesis. Proc R Soc Lond B Biol Sci. 1971; 177: 109-159.
8. Chatzizisis YS, Jonas M, Coskun AU, Beigel R, Stone BV, Maynard C, et al. Prediction of the localization of high-risk coronary atherosclerotic plaques on the basis of low endothelial shear stress: an intravascular ultrasound and histopathology natural history study. Circulation. 2008; 117: 993-1002.
9. Frydrychowicz A, Stadler AF, Russe MF, Bock J, Bauer S, Harloff A, et al. Three-dimensional analysis of segmental wall shear stress in the aorta by flow-sensitive four-dimensional-MRI. J Magn Reson Imaging. 2009; 30: 77-84.
10. Knight J, Olgac U, Saur SC, Poulikakos D, Marshall W Jr, Cattin PC, et al. Choosing the optimal wall shear parameter for the prediction of plaque location-A patient-specific computational study in human right coronary arteries. Atherosclerosis. 2010; 211: 445-450.
11. Moore JA, Steinman DA, Holdsworth DW, Ethier CR. Accuracy of computational hemodynamics in complex arterial geometries reconstructed from magnetic resonance imaging. Ann Biomed Eng. 1999; 27: 32-41.
12. Steinman DA. Image-based computational fluid dynamics modeling in realistic arterial geometries. Ann Biomed Eng. 2002; 30: 483-497.
13. Steinman DA, Milner JS, Norley CJ, Lownie SP, Holdsworth DW. Image-based computational simulation of flow dynamics in a giant intracranial aneurysm. AJNR Am J Neuroradiol. 2003; 24: 559-566.
14. Kleinstreuer C. Biofluid dynamics, Principles and selected applications, Taylor & Francis, New York, 2006.
15. ANSYS Fluent 14.0. Documentation, ANSYS Inc. Canonsburg, PA, USA, http://www.ansys.com, 2012.
16. Soulis JV, Giannoglou GD, Chatzizisis YS, Seralidou KV, Parcharidis GE, Louridas GE. Non-Newtonian models for molecular viscosity and wall shear stress in a 3D reconstructed human left coronary artery. Med Eng Phys. 2008, 30: 9–19.
17. Soulis JV, Fytanidis DK, Papaioannou VC, Styliadis H, Giannoglou GD. Oscillating LDL accumulation in normal human aortic arch - shear dependent endothelium. Hippokratia. 2011; 15: 22-25.
18. Murray CD. The Physiological Principle of Minimum Work. I. The Vascular System and the Cost of Blood Volume. Proc Natl Acad Sci U S A. 1926, 12: 207-214.
19. Himburg HA, Grzybowski DM, Hazel AL, LaMack AL, Li XM, Friedman MH. Spatial comparison between wall shear stress measures and porcine arterial endothelial permeability. Am J Physiol Heart Circ Physiol.2004, 286: H1916-H1922.
20. Wen CY, Yang AS, Tseng LY, Chai JW. Investigation of pulsatile flow field in healthy thoracic aorta models. Ann Biomed Eng. 2009, 38: 391-402.
21. Lantz J, Gårdhagen R, Karlsson M. Quantifying turbulent wall shear stress in a subject specific human aorta using large eddy simulation. Med Eng Phys. 2012; 34: 1139-1148.
22. Tang BT, Fonte TA, Chan FP, Tsao PS, Feinstein JA, Taylor CA. Three-dimensional hemodynamics in the human pulmonary arteries under resting and exercise conditions. Ann Biomed Eng. 2011; 39: 347-358.